Iron Oxidation State Modulates Active Site Structure in a Heme Peroxidase[†,‡]

Sandip K. Badyal,[§] Clive L. Metcalfe,[§] Jaswir Basran,[||] Igor Efimov,[§] Peter C. E. Moody,[||] and Emma Lloyd Raven*[,§]

Department of Chemistry, Henry Wellcome Building, University of Leicester, University Road, Leicester LE1 7RH, England, U.K., and Department of Biochemistry and Henry Wellcome Laboratories for Structural Biology, Henry Wellcome Building, University of Leicester, Lancaster Road, Leicester LE1 9HN, England, U.K.

Received November 27, 2007; Revised Manuscript Received February 14, 2008

ABSTRACT: We have previously shown [Badyal, S. K., et al. (2006) *J. Biol. Chem. 281*, 24512–24520] that the distal histidine (His42) in the W41A variant of ascorbate peroxidase binds to the heme iron in the ferric form of the protein but that binding of the substrate triggers a conformational change in which His42 dissociates from the heme. In this work, we show that this conformational rearrangement also occurs upon reduction of the heme iron. Thus, we present X-ray crystallographic data to show that reduction of the heme leads to dissociation of His42 from the iron in the ferrous form of W41A; spectroscopic and ligand binding data support this observation. Structural evidence indicates that heme reduction occurs through formation of a reduced, bis-histidine-ligated species that subsequently decays by dissociation of His42 from the heme. Collectively, the data provide clear evidence that conformational movement within the same heme active site can be controlled by both ligand binding and metal oxidation state. These observations are consistent with emerging data on other, more complex regulatory and sensing heme proteins, and the data are discussed in the context of our developing views in this area.

The iron-containing heme group is used widely in biology. Traditionally, heme-containing proteins have been categorized into the oxygen transport proteins (the globins), the electron transfer proteins (the cytochromes), and the catalytic heme-containing enzymes (e.g., the P450s, peroxidases, etc.). This categorization conveniently differentiated the noncatalytic electron transfer proteins from the transport proteins and the catalytic enzymes, and it became clear that at least part of this differentiation arose from differences in heme coordination geometry. Hence, the electron transfer proteins contain six-coordinated heme groups, as a means of facilitating rapid electron transfer, whereas the transport proteins and the catalytic enzymes are most often found as five-coordinate or weakly six-coordinate heme structures to allow ligand binding or catalysis at the sixth site. Over the past several years, a few examples emerged in the literature of heme proteins that did not fit this categorization. This was because these proteins actually switched their heme coordination geometry through conformational rearrangements of the protein structure. Examples include cytochrome *c* (*1*), *Chlamydomonas* hemoglobin (*2*), cytochrome cd_1 (*3*), the diheme cytochrome *c* peroxidase (*4*), the heme chaperone protein CcmE (*5*), and leghemoglobin (*6*). The trigger for these conformational rearrangements appeared to be, variously, pH, the oxidation state of the iron, and the binding of ligands, substrate, or other (noncatalytic) metal ions. Although these documented examples were significant in their own right, their collective significance was not immediately apparent. This was in part because a functional basis for the ligand switch could not be identified in all cases. Later, further examples of conformational rearrangements in other regulatory heme proteins linked to, for example, gas-sensing processes, signaling, and gene transcription were published (see ref *7* for a recent review). It was only then that it started to become clear that conformational rearrangements associated with the heme group, its ligands and/or substrates, and its oxidation state might actually be used more widely as a means of regulation and/or sensing in biology.

Currently, therefore, it appears that at least some heme protein architectures are intrinsically mobile, that this mobility can be triggered by redox changes or ligand−substrate binding, and that this trigger is used, in certain cases, as a link to more complex downstream biological processes. What we do not yet know is whether conformational mobility is a more general characteristic of other heme protein structures and whether these triggering mechanisms are more generally accessible in other protein structures. In this context, we have recently reported (*8*) an example of a six-coordinate heme peroxidase (W41A variant of ascorbate peroxidase) which has bis-histidine coordination, like a cytochrome, but that is catalytically active because the distal histidine reversibly dissociates to form a five-coordinate heme in response to binding of hydrogen peroxide. In this work, we show that this conformational movement is also triggered by a change in oxidation state. The implications of these observations are

[†] This work was supported by grants from the BBSRC (Grants BB/C00602X/1, BB/C001184/1, and IIP0206/009, and a studentship to S.K.B.) and ESRF Proposal MX-635.

[‡] PDB accession codes for the protein structures reported in this paper are as follows: 2VNZ (ferrous W41A), 2VO2 (low-dose W41A), and 2VNX (high-dose W41A).

* To whom correspondence should be addressed. Telephone: +44 (0)116 2297047. Fax: +44 (0)116 2522789. E-mail: emma.raven@le.ac.uk.

[§] Department of Chemistry, University of Leicester.

[||] Department of Biochemistry and Henry Wellcome Laboratories for Structural Biology, University of Leicester.

10.1021/bi702337n CCC: $40.75
Published on Web 03/20/2008

discussed in terms of our evolving understanding of the role of heme in biological regulation and sensing.

EXPERIMENTAL PROCEDURES

Materials. Sodium dithionite, sodium azide, and potassium cyanide were purchased from Sigma-Aldrich, and the chemicals used for buffers (Fisher) were of the highest analytical grade (>99% pure) and were used without further purification. Aqueous solutions were prepared using water purified through an Elgastat Option 2 water purifier, which itself was fed with deionized water. All pH measurements were made using a Russell pH electrode attached to a digital pH meter (Radiometer Copenhagen, model PHM 93).

Protein Expression and Purification. Bacterial fermentation of cells and purification of rsAPX[1] and W41A were carried out according to published procedures (*8, 9*). Purified samples of rsAPX and W41A exhibited wavelength maxima at 407 (107), 525, and ≈630 nm and 405 (125), 525, 564, and ≈630 nm, respectively, as reported previously (*8, 10*). Enzyme concentrations for rsAPX and W41A were determined using the following absorption coefficients: $\epsilon_{407} = 107$ mM^{-1} cm^{-1} (*10*) and $\epsilon_{405} = 125$ mM^{-1} cm^{-1} (*8*), respectively.

Electronic Absorption Spectroscopy. Spectra were collected using a Perkin-Elmer Lambda 25, 35, or 40 spectrophotometer, linked to a PC workstation running UV-Winlab. Ferrous forms of rsAPX and W41A were prepared by the addition of microliter volumes of a fresh sodium dithionite solution to the ferric enzyme (~8 μM) present in anaerobic buffer in an airtight cuvette until no further change in the spectrum was observed. All solutions were prepared in a glovebox (Belle Technology) using anaerobic buffer.

Titrations with Anionic Ligands. Equilibrium binding parameters were determined by adding microliter volumes of the appropriately diluted ligand (cyanide or azide) solutions (made up in sodium phosphate buffer, pH 7.0, $\mu = 0.1$ M, and filter-sterilized) using a Hamilton syringe to an airtight cuvette containing ferric protein, which was mixed by inversion and allowed to equilibrate. The UV–visible spectra (270−700 nm) were recorded after each addition of ligand. The ligand binding affinity was monitored spectroscopically using absorption at 418 nm for cyanide binding to rsAPX and W41A and 411.5 and 405 nm for azide binding to rsAPX and W41A, respectively.

All solutions for determining parameters for binding of cyanide to ferrous protein were prepared anaerobically in a glovebox, by the addition of microliter volumes of a fresh sodium dithionite solution to an anaerobic solution of ferric protein (~8 μM) until no further change in the spectrum was observed. All solutions required for the titrations were kept anaerobic by the use of glucose (Fisher, 10 mM), glucose oxidase (Sigma, 50 μg/mL), and catalase (Sigma, 5 μg/mL). The same method that was described above for the ferric form was used for the titration of cyanide into dithionite-reduced protein. The ligand binding affinity was monitored spectroscopically using absorption at 426 nm for cyanide binding to reduced rsAPX and W41A. As a consequence of the high affinity of ferric rsAPX for cyanide, a nonlinear regression analysis using eq 1 was applied to determine the K_d

$$\Delta A = \frac{\Delta A_\infty}{2[E]}\{[E] + [L] + K_d - [([E] + [L] + K_d)^2 - 4[E][L]]^{1/2}\} \quad (1)$$

where [E] and [L] represent the calculated concentrations of total enzyme and total ligand after each addition, respectively, ΔA and ΔA_∞ are the absorbance changes corresponding to the intermediate and saturating ligand concentrations, respectively, and K_d is the equilibrium dissociation constant.

Equilibrium dissociation constants for binding of cyanide to ferrous rsAPX and ferric/ferrous W41A, and of azide to ferric rsAPX and W41A, were calculated using eq 2 in Grafit 5 (Grafit version 5.0.3, Erithacus Software Ltd.):

$$\Delta A = \frac{\Delta A_\infty[\text{free}]}{K_d + [\text{free}]} \quad (2)$$

where ΔA and ΔA_∞ are the absorbance changes corresponding to the intermediate and saturating ligand concentrations, respectively, [free] is total concentration of unbound ligand, and K_d is the equilibrium dissociation constant.

Transient-State Kinetics. Transient-state measurements were performed using an SX.18MV microvolume stopped-flow spectrophotometer (Applied Photophysics) contained within a glovebox (Belle Technology) and fitted to a Neslab RTE-200 circulating water bath (5 ± 0.1 °C). Multiple-wavelength absorption studies were carried out using a photodiode array detector and X-SCAN (Applied Photophysics Ltd.). Spectral deconvolution was performed by global analysis and numerical integration methods using PROKIN (Applied Photophysics Ltd.).

Crystal Growth and Structure Determination. Crystals of W41A were obtained using previously published procedures (*11*). Crystals of ferrous W41A were obtained by soaking crystals for 5 min in a fresh solution of sodium dithionite dissolved in mother liquor [0.1 M Hepes (pH 8.3) and 2.25 M lithium sulfate]. All crystals were flash-frozen and then cryocooled in liquid nitrogen and stored for data collection.

All diffraction data were collected at ESRF (Grenoble, France) for dithionite-reduced W41A using beam line ID23-EH1 (0.873Å) and an ADSC Quantum-315 detector. Single-crystal microspectrometry and collection of diffraction before and after X-ray reduction of ferric W41A used beamline ID14-2 (0.933Å) and an ADSC Q4 CCD detector. All synchrotron data were collected at 100 K. The data were indexed and scaled using MOSFLM (*12*) and SCALA (*13*). Crystals were continuously cooled by a cold nitrogen stream from an Oxford Cryosystems 700 series cryostream. UV−visible absorption spectra of the crystals were recorded in the 500–800 nm range using the EMBL online microspectrophotometer (HR2000 CCD detector Ocean Optics). Input light was provided by a deuterium/halogen source (Ocean Optics, DH2000) coupled to custom lenses via a 100 μm 2-UV-SR fiber optic (generating a focal spot of 25 μm) and collected from the second lens coupled to a 600 um fiber optic. Wherever possible, care was taken to record spectra of the crystal to the same φ position. Spectra of the cryocooled crystals remained unchanged during storage.

[1] Abbreviations: APX, ascorbate peroxidase; rsAPX, recombinant soybean cytosolic ascorbate peroxidase.

Table 1: Data Collection and Refinement Statistics[a]

	ferrous	low-dose	high-dose
Data Collection			
PDB entry	2VNZ	2VO2	2VNX
space group	$P4_22_12$	$P4_22_12$	$P4_22_12$
unit cell dimensions (Å)			
$a = b$	81.78	82.06	82.00
c	75.24	75.63	75.57
resolution (Å)	45.83–1.30 (1.39–1.30)	46.03–2.00 (2.11–2.00)	37.80–1.60 (1.69–1.60)
total no. of observations	649696 (94551)	63697 (9264)	352976 (49343)
no. of unique reflections	63112 (9091)	17935 (2570)	34661 (4988)
$I/\sigma I$	21.6 (4.3)	6.2 (0.9)	19.5 (3.1)
R_{merge}	0.09 (0.45)	0.026 (0.138)	0.086 (0.66)
completeness (%)	99.9 (100)	99.7 (100)	100 (100)
Refinement Statistics			
R_{work}	0.182	0.174	0.175
R_{free}	0.199	0.236	0.209
root-mean-square deviations from ideal			
bonds (Å)	0.006	0.016	0.010
angles (deg)	1.117	1.507	1.152

[a] Values in parentheses are for the outer shell.

Data collection and processing statistics are listed in Table 1; 5% of the data was flagged for the calculation of R_{free} and excluded from subsequent refinement. The structures were refined from the 1.35 Å ferric W41A structure (Protein Data Bank entry 2GGN). Several cycles of refinement using REFMAC5 (*14*) from the CCP4 suite (*13*) and manual rebuilding of the protein model using COOT (*15*) followed by the addition of water molecules were carried out until the R_{free} and R_{factor} values converged. The final refinement statistics are presented in Table 1.

RESULTS AND DISCUSSION

Spectra of Ferric and Ferrous Derivatives. The electronic spectra of the ferric and ferrous derivatives of rsAPX and W41A are shown in Figure 1. The spectrum of the ferric derivative of W41A [λ_{max} = 405 (ϵ = 125 mM^{-1} cm^{-1}), 525, 564, and 630 nm] (*8*) shows a peak in the visible region (564 nm) that is consistent with the presence of low-spin heme (Figure 1B). This distinguishes it clearly from the spectrum of ferric rsAPX (Figure 1A) in which no low-spin peaks are observed [λ_{max} = 407 (ϵ = 107 mM^{-1} cm^{-1}), 525, and ≈630 nm (ϵ = 16 mM^{-1} cm^{-1})]. For W41A, the low-spin component has been shown, crystallographically, to derive from coordination of the distal histidine (His42) to the ferric heme (*8*). In contrast, the spectra of the ferrous derivatives of rsAPX and W41A (Figure 1A,B) are similar to each other (λ_{max} = 430, 555, and 583 nm for rsAPX; λ_{max} = 428, 556, and 581 nm for W41A), with both spectra consistent with a reduced heme species. As reduced rsAPX is five-coordinate, this suggests that in the dithionite-reduced form of W41A the His42 ligand dissociates from the iron.

Ligand Binding to Ferric and Ferrous Derivatives. Complete formation of low-spin ferric heme is observed upon addition of cyanide to both ferric rsAPX [λ_{max} = 419, 536, and 563^{sh} nm (data not shown)] and W41A [λ_{max} = 418, 540, and 561^{sh} nm (Figure 1C)]. This is consistent with binding of cyanide at the sixth coordination site, as confirmed crystallographically in both cases (*8*). Addition of azide to ferric rsAPX and W41A leads to a predominantly low-spin ferric heme species with some high-spin character [λ_{max} = 412, 528^{sh}, 562^{sh}, and 630 nm for rsAPX; λ_{max} = 415, 538^{sh},

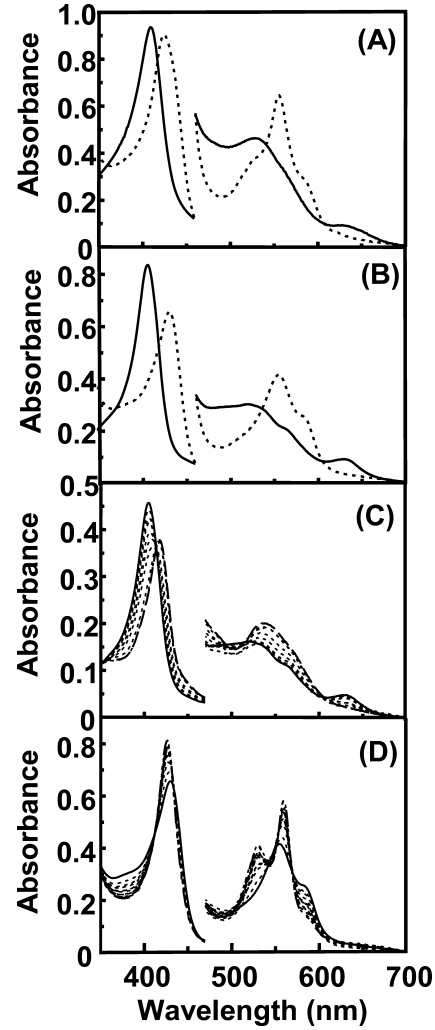

FIGURE 1: Electronic spectra of (A) rsAPX and (B) W41A, showing the ferric (solid line) and ferrous (dashed line) species. The ferrous spectra were obtained by addition of dithionite. (C and D) Selected spectra collected during titration of (C) ferric W41A (3.6 μM) and (D) ferrous W41A (6.8 μM) with cyanide. Intermediate spectra between the initial spectrum (solid line) and the final saturated spectrum (dashed line) are shown as dotted lines. Sample conditions: enzyme, sodium phosphate, pH 7.0, μ = 0.1 M, 25 °C. The visible region has been multiplied by a factor of 5 in all cases.

Table 2: Equilibrium Dissociation Constants for Binding of Cyanide and Azide to rsAPX and W41A[a]

	rsAPX		W41A	
	ferric	ferrous	ferric	ferrous
cyanide	0.73 ± 0.075 μM	0.31 ± 0.025 mM	20 ± 0.75 μM	1.5 ± 0.17 mM
azide	0.40 ± 0.019 mM	–	3.8 ± 0.091 mM	–

[a] Sample conditions: sodium phosphate, pH 7.0, μ = 0.1 M, 25 °C.

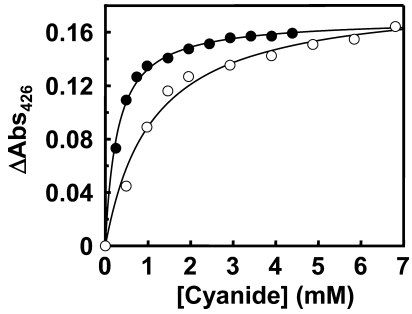

FIGURE 2: Plot of the absorbance change at 426 nm vs total cyanide concentration for binding to ferrous rsAPX (●) and ferrous W41A (○). The solid line is a fit of the data to eq 2.

562[sh], and 630 nm for W41A (data not shown)]. Similarly, addition of potassium cyanide to ferrous rsAPX and W41A leads to formation of a low-spin species in both cases [λ_{max} = 426, 529, and 560 nm for rsAPX (data not shown); λ_{max} = 426, 530, and 560 nm for W41A (Figure 1D)].

Equilibrium binding constants (Table 2 and Figure 2) obtained from the data given above showed large differences in the binding affinity between the ferric forms of rsAPX and W41A, with K_d values for binding of cyanide and azide ≈30- and ≈10-fold lower, respectively, for W41A than those for rsAPX. This can be rationalized by the different coordination geometries in the two proteins: rsAPX contains a weakly bound water molecule at the sixth coordination position, whereas in W41A, the distal histidine binds to the heme at the sixth site. In contrast, binding constants for binding of cyanide to the ferrous form are closely matched for both rsAPX and W41A (Table 2). This is consistent with the electronic spectra of the ferrous forms of the two proteins and indicates that the coordination geometry is similar in both cases.

Crystallography. The crystal structure of ferric W41A [Figure 3A (*8*)] indicated that His42 was within bonding distance (2.3 Å, compared to 5.5 Å in rsAPX) of the iron, to give six-coordinate heme. We have called this the "on" form (*8*). The crystal structure of the dithionite-reduced form of W41A (Figure 3B and Table 1) reveals that His42 is no longer bound to the iron and shows a water molecule in the active site (Fe−O distance of 2.12 Å). Although the overall structure of ferrous W41A is similar to that of ferric W41A, there are changes in conformation around His42. Hence, the main chain of His42 in ferrous W41A has moved away from the heme to a position analogous to that of His42 in the structure of ferric rsAPX. We have referred to this conformation of His42 as the "off" form. For dithionite-reduced W41A, there is no additional density directly above the iron that correlates to the histidine being ligated to the iron (i.e., in the on form); the only density is for the water molecule as described above.

Reduction of the heme is also possible during collection of crystallographic data (see, for example, refs *17*–*20*), and

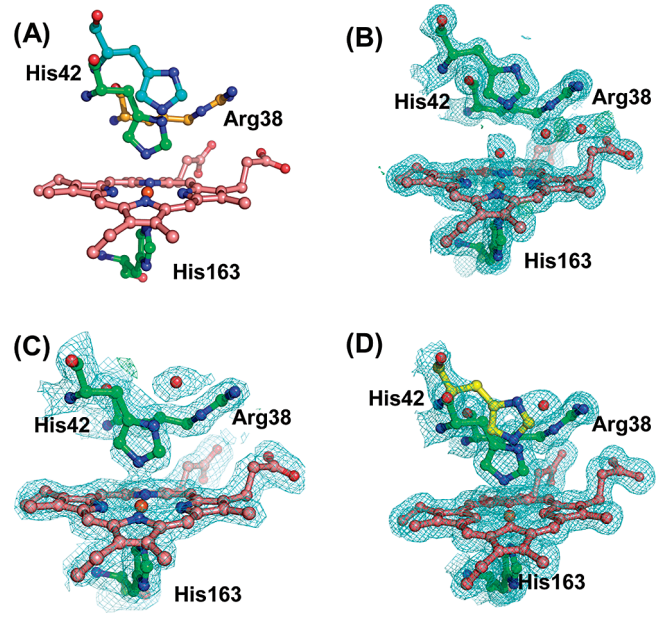

FIGURE 3: (A) Structural alignment of the active sites of rsAPX (blue, Protein Data Bank entry 1OAG) and W41A (green), showing the orientation of His42 in the off and on positions, respectively. Arg38 is highlighted in yellow. (B) Structure of W41A after reduction by dithionite, showing His42 in the off position. (C) Structure of W41A after exposure to low-intensity irradiation. (D) Structure of W41A after exposure to high-intensity irradiation showing the dual occupancy of His42. The σA-weighted $2F_o - F_c$ electron density at 1σ is colored blue. The off position of His42 is colored yellow (modeled with an occupancy of 0.3), and the on position of His42 is colored green (modeled with an occupancy of 0.7). This figure was created using PyMOL (*30*). Water molecules are shown as red spheres in all cases.

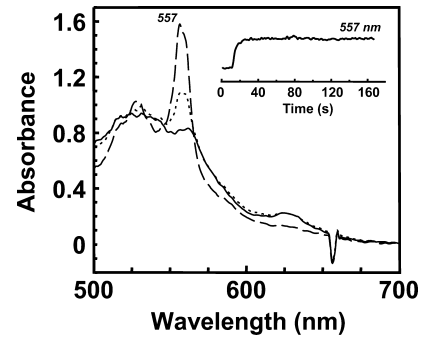

FIGURE 4: Changes in the absorption spectrum (100 K) of a crystal of ferric W41A (solid line) on exposure to small (dotted line) and large (dashed line) X-ray doses. The inset is a plot showing the time-dependent changes in absorbance at 557 nm on exposure of the crystal to a high-intensity X-ray beam.

we used this to obtain further structural evidence for movement of His42 between the on and off positions. The structures of a crystal of ferric W41A determined after exposure to an attenuated-low intensity X-ray source (low-dose) and the full-intensity unattenuated X-ray source (high-dose) are shown in panels C and D of Figure 3, respectively.

Scheme 1: Species Observed in This and Previous (*8*) Work, Showing the Mobility of His42 during Catalysis and Reduction[a]

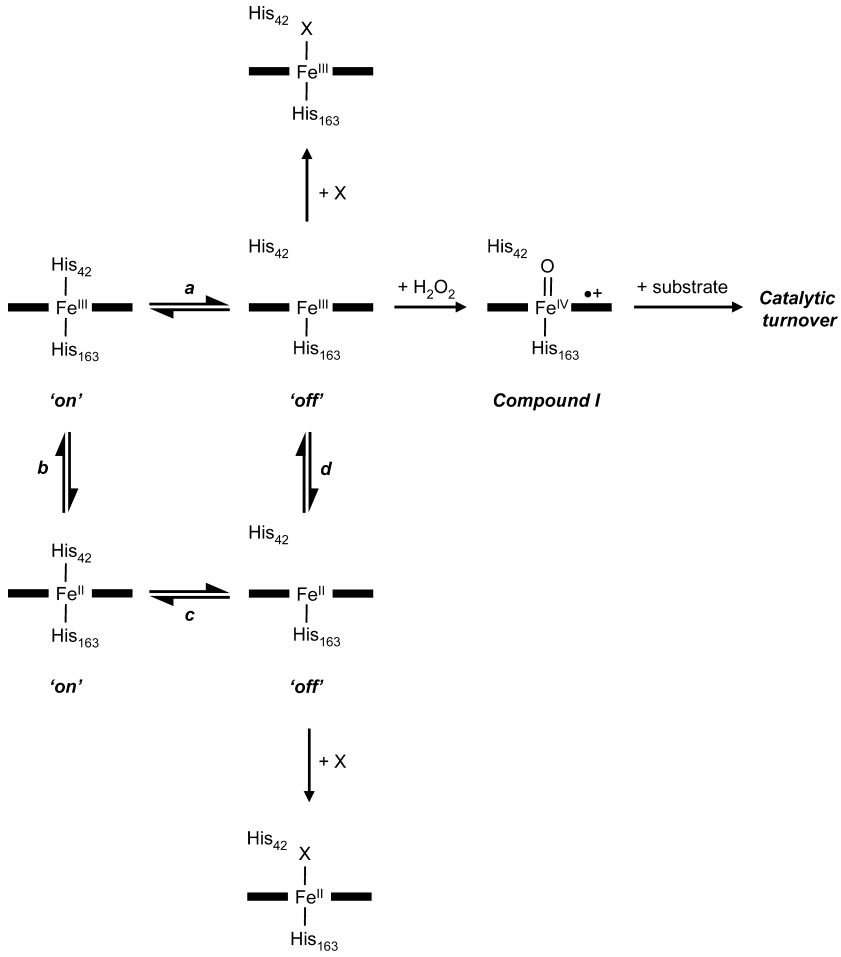

[a] Step a shows the equilibrium between the on and off forms of the ferric protein. This form has been previously shown (*8*) to bind both exogenous ligands and to be catalytically active (reaction with H_2O_2), as shown herein. Step b represents the reduction of ferric W41A to an initial low-spin ferrous form, which is the likely route in the X-ray beam. Step c represents subsequent loss of His42 from this initial low-spin ferrous intermediate; this form can also bind exogenous ligands. Step d shows the reoxidation of the ferrous off form to the ferric form. On reaction with dithionite in solution, step b followed by c is possible, but an alternative mechanism in which reduction of the ferrous form with dithionite involves prior dissociation of His42 from the heme before reduction (step a followed by step d) is also possible.

The structure for the low-dose sample (Figure 3C) is similar to that of pure ferric W41A (Figure 3A), in which His42 is in the on position and within bonding distance (2.3 Å) of the iron, and there is no additional density above the heme corresponding to the off position. In contrast, for the high-dose structure, there is positive $F_o - F_c$ density above His42, near the main chain of His42 and close to the off position. This second conformation [which is not observed at low X-ray doses (Figure 3C)] was refined placing His42 in an orientation identical to that of His42 in dithionite-reduced ferrous W41A (Figure 3B). The occupancies of the two conformations were estimated to be 0.3 for the off form and 0.7 for the on form and included in the final stages of refinement; the resulting electron density is shown in Figure 3D. Thus, on exposure to the high-dose beam, the ferric W41A crystal is being reduced and His42 is observed to partially move away from the iron on reduction.

In parallel experiments, single-crystal microspectrophotometry was used to monitor changes in the electronic spectrum of the ferric W41A crystal that correspond to the structures presented in Figure 3. The initial spectrum of the ferric W41A crystal at 100 K (Figure 4) before exposure to the beam is the same as that observed in solution at room temperature (Figure 1B). This indicates that the species in solution and in the crystal are similar and demonstrates that freezing and crystallization effects are not responsible for the conformational movement. [In fact, we note that the bond in the on form (2.3 Å) is longer than usual for an iron−histidine bond, which accounts for the 630 nm (high-spin) band in the visible region at both room temperature and 100 K and suggests that His42 is quite weakly coordinated.] When the ferric W41A crystal was exposed to a low-intensity beam, an increase in absorbance at 557 nm [close to the absorption maximum for the ferrous derivative (Figure 1)] was observed (Figure 4). Note, however, that no additional density was observed for His42 in the off position in the corresponding structure of this species (Figure 3C), indicating that under these conditions His42 is not yet dissociated from the iron even though a significant population of the heme groups have been reduced by the beam, as evidenced by the change in absorbance at 557 nm. On exposure of the ferric W41A crystal to a high-intensity X-ray beam, much larger increases in absorbance at 557 nm are observed over time (Figure 4 and inset) so that the final spectrum after data collection resembled that of a ferrous bis-histidine (low-spin) heme species, such as

cytochrome b_5 (*21*). The structure that corresponds to this reduced spectrum (Figure 3D) clearly shows His42 still within bonding distance of the iron, but there is additional density above His42 in the off position. Reduction of the ferric crystal was complete within ~40 s at 100 K (Figure 4 inset). Significantly, the final spectrum after 40 s is different from that obtained when W41A is chemically reduced by dithionite (Figure 1B). This is interpreted as evidence that reduction of ferrous W41A in the beam at 100 K leads to an initial reduced, bis-histidine species which presumably then decays back to a species that is the same as that observed when W41A is reduced with dithionite in solution. In transient-state kinetic experiments (photodiode array stopped flow, 5 °C), there was no evidence of the presence of a bis-histidine ligated ferrous heme protein in solution on reaction of W41A with dithionite (data not shown), and we assume that at this temperature the conformational rearrangements occur more rapidly so that the reduced, bis-histidine species decays too quickly for detection by stopped flow.

Wider Implications. There are relatively few examples of crystallographically defined conformational changes in heme proteins. In previous work (*8*), we showed that the coordination geometry in W41A was variable so that His42 binds onto the heme in the oxidized form but that addition of peroxide triggered a conformational change that led to displacement of His42 so that essentially complete catalytic activity was maintained. This ran counter to widely adopted views of heme enzyme catalysis, because it showed that strong coordination of His42 to the heme does not, automatically, undermine catalytic activity.

The data presented above show that a conformational movement within the protein structure can also be triggered by a change in the oxidation state of the iron, and we present crystallographic evidence to show dissociation of His42 on reduction. The major findings are summarized in Scheme 1. On the basis of the data presented, we propose a mechanism for reduction that involves initial formation of a reduced, bis-histidine-ligated species that subsequently decays by dissociation of His42 from the heme. What is clear is that conformational mobility can be induced within the same protein structure either by ligand (peroxide) binding (*8*) or by reduction of the heme. As noted above, other examples of conformationally mobile heme protein structures have appeared sporadically (for example, refs *1–5* and *22*). Collectively, we interpret this as evidence that these protein structures are intrinsically mobile and that this might be a feature of other heme protein structures that is used more widely than previously realized.

These observations chime with our developing views on the wider role of heme in biological systems because it is now becoming clear that the role of heme is not restricted to its involvement as a prosthetic group in specific proteins and enzymes but that it is also involved in various regulatory processes, including gas sensing, control of gene transcription, and modulation of ion channels. The limited information that is currently available seems to suggest that the trigger for these regulatory processes is similarly controlled either by ligand binding or by the oxidation state of the iron and that either of these events is used to initiate downstream conformational rearrangements of the protein architecture either at the active site or beyond. Examples include ligand binding to the heme-regulated inhibitor kinase (*23*) and the heme sensor HemAT (*24*), and reduction of the iron in the heme-regulated phosphodiesterase from *Escherichia coli* (*25*) and in CooA (*26, 27*). Similar mechanisms might also apply to gas-responsive transcription factor NPAS2 (*28*), heme-binding transcription factor Hap1 (*29*), and heme-based sensor FixL (*30*).

ACKNOWLEDGMENT

We thank Dr. John McGeehan for support in using the microspectrophotometer on ID14-2. We are grateful to Dr. Klaus Futterer for collection of the ferrous W41A crystal data. We also thank Dr. Louise Fairall and Dr. Alexandre R. Gingras for assistance with graphics.

REFERENCES

1. Rosell, F. I., Ferrer, J. C., and Mauk, A. G. (1998) Proton-Linked Protein Conformational Switching: Definition of the Alkaline Conformational Transition of Yeast Iso-1-ferricytochrome c. *J. Am. Chem. Soc. 120*, 11234–11245.
2. Das, K. T., Couture, M., Lee, H. C., Peisach, J., Rousseau, D. L., Wittenberg, B. A., Wittenberg, J. B., and Guertin, H. (1999) Identification of the Ligands to the Ferric Heme of *Chlamydomonas* Chloroplast Hemoglobin: Evidence for Ligation of Tyrosine-63 (B10) to the Heme. *Biochemistry 38*, 15360–15368.
3. Williams, P. A., Fulop, V., Garman, E. F., Saunders, N. F. W., Ferguson, S. J., and Hajdu, J. (1997) Haem ligand-switching during catalysis in crystals of a nitrogen cycle enzyme. *Nature 389*, 406–412.
4. Dias, J. M., Alves, T., Bonoifacio, C., Pereira, A. S., Trincao, J., Bougeois, D., Moura, I., and Romano, M. (2004) Structural Basis for the Mechanism of Ca^{2+} Activation of the Di-Heme Cytochrome c Peroxidase from Pseudomonas nautica 617. *Structure 12*, 961–973.
5. Uchida, T., Stevens, J. M., Daltrop, O., Harvat, E. M., Hong, L., Ferguson, S. J., and Kitagawa, T. (2004) The interaction of covalently bound heme with the cytochrome c maturation protein CcmE. *J. Biol. Chem. 279*, 51981–51988.
6. Patel, N., Jones, D. K., Cheesman, M. R., Thomson, A. J., and Raven, E. L. (2002) Leghaemoglobin: A model for the investigation of haem protein axial ligation. *Inorg. Chim. Acta,* 303–309.
7. Poulos, T. L. (2007) The Janus nature of heme. *Nat. Prod. Rep. 24*, 504–510.
8. Badyal, S. K., Joyce, M. G., Sharp, K. H., Seward, H. E., Mewies, M., Basran, J., Macdonald, I. K., Moody, P. C. E., and Raven, E. L. (2006) Conformational mobility in the active site of a heme peroxidase. *J. Biol. Chem. 281*, 24512–24520.
9. Metcalfe, C. L., Ott, M., Patel, N., Singh, K., Mistry, S. C., Goff, H. M., and Raven, E. L. (2004) Autocatalytic formation of green heme: Evidence for H_2O_2-dependent formation of a covalent methionine-heme linkage in ascorbate peroxidase. *J. Am. Chem. Soc. 126*, 16242–16248.
10. Jones, D. K., Dalton, D. A., Rosell, F. I., and Raven, E. L. (1998) Class I heme peroxidases: Characterization of soybean ascorbate peroxidase. *Arch. Biochem. Biophys. 360*, 173–178.
11. Sharp, K. H., Mewies, M., Moody, P. C. E., and Raven, E. L. (2003) Crystal structure of the ascorbate peroxidase-ascorbate complex. *Nat. Struct. Biol. 10*, 303–307.
12. Leslie, A. G. W. (1992) Recent changes to the MOSFLM package for processing film and image plate data. *Joint CCP4 + ESF-EAMCB Newsletter on Protein Crystallography 26*, 134–135.
13. Collaborative Computational Project Number 4 (1994) The CCP4 suite: Programs for protein crystallography. *Acta Crystallogr. D50*, 760–763.
14. Murshudov, G. N., Vagin, A. A., and Dodson, E. J. (1997) Refinement of Macromolecular Structures by the Maximum-Likelihood Method. *Acta Crystallogr. D53*, 240–255.
15. Emsley, P., and Cowtan, K. (2004) *Acta Crystallogr. D60*, 2126–2132.
16. Lad, L., Mewies, M., and Raven, E. L. (2002) Substrate Binding and Catalytic Mechanism in Ascorbate Peroxidase: Evidence for Two Ascorbate Binding Sites. *Biochemistry 41*, 13774–13781.
17. Berglund, G. I., Carlsson, G. H., Smith, A. T., Szoke, H., Henriksen, A., and Hajdu, J. (2002) The catalytic pathway of horseradish peroxidase at high resolution. *Nature 417*, 463–468.

18. Hersleth, H. P., Dalhus, B., Gorbitz, C. H., and Andersson, K. K. (2002) An iron hydroxide moiety in the 1.35 angstrom resolution structure of hydrogen peroxide derived myoglobin compound II at pH 5.2. *J. Biol. Inorg. Chem. 7*, 299–304.
19. Schlichting, I., Berendzen, J., Chu, K., Stock, A. M., Maves, S. A., Benson, D. E., Sweet, R. M., Ringe, D., Petsko, G. A., and Sligar, S. G. (2000) The catalytic pathway of cytochrome P450cam at atomic resolution. *Science 287*, 1615–1622.
20. Hersleth, H. P., Uchida, T., Rohr, A. K., Teschner, T., Schunemann, V., Kitagawa, T., Trautwein, A. X., Gorbitz, C. H., and Andersson, K. K. (2007) Crystallographic and spectroscopic studies of peroxide-derived myoglobin compound II and occurrence of protonated $Fe^{IV}O$. *J. Biol. Chem. 282*, 23372–23386.
21. Ozols, J., and Strittmatter, P. (1964) The Interaction of Porphyrins and Metalloporphyrins with Apocytochrome b_5. *J. Biol. Chem. 239*, 1018–1023.
22. Patel, N., Seward, H. E., Svensson, A., Gurman, S. J., Thomson, A. J., and Raven, E. L. (2003) Exploiting the conformational flexibility of leghemoglobin: A framework for examination of heme proetin axial ligation. *Arch. Biochem. Biophys. 418*, 197–204.
23. Igarashi, J., Sato, A., Kitagawa, T., Yoshimura, T., Yamauchi, S., Sagami, I., and Shimizu, T. (2004) Activation of Heme-regulated Eukaryotic Initiation Factor 2α Kinase by Nitric Oxide Is Induced by the Formation of a Five-coordinate NO-Heme Complex. *J. Biol. Chem. 279*, 15752–15762.
24. Pinakoulaki, E., Yoshimura, H., Daskalakis, V., Yoshioka, S., Aono, S., and Varotsis, C. (2006) Two ligand-binding sites in the O_2-sensing signal transducer HemAT: Implications for ligand recognition/discrimination and signaling. *Proc. Natl. Acad. Sci. U.S.A. 103*, 14796–14801.
25. Kurokawa, H., Lee, D. S., Watanabe, M., Sagami, I., Mikami, B., Raman, C. S., and Shimizu, T. (2004) A redox controlled molecular switch revealed by the crystal structure of a bacterial heme PAS sensor. *J. Biol. Chem. 279*, 20186–20193.
26. Lanzilotta, W. N., Schuller, D. J., Thorstensson, M. V., Kerby, R. L., Roberts, G. P., and Poulos, T. L. (2000) Structure of the CO sensing transcription activator CooA. *Nat. Struct. Biol. 7*, 876–880.
27. Nakajima, H., Honma, Y., Tawara, T., Kato, T., Park, S. Y., Miyatake, H., Shiro, Y., and Aono, S. (2001) Redox Properties and Coordination Structure of the Heme in the CO-sensing Transcriptional Activator CooA. *J. Biol. Chem. 276*, 7055–7061.
28. Dioum, E. M., Rutter, J., Tuckerman, J. R., Gonzalez, G., Gilles-Gonzalez, M.-A., and McKnight, S. L. (2002) NPAS2: A gas-repsonsive transcription factor. *Science 298*, 2385–2387.
29. Lan, C., Lee, H. C., Tang, S., and Zhang, L. (2004) A novel mode of chaperon action. *J. Biol. Chem. 279*, 27607–27612.
30. Gilles-Gonzalez, M. A., and Gonzalez, G. (2005) Heme-based sensors: Defining characteristics, recent developments, and regulatory hypotheses. *J. Inorg. Biochem. 99*, 1–22.

BI702337N